DOI 10.1007/s11182-016-0679-x

Russian Physics Journal, Vol. 58, No. 11, March, 2016 (Russian Original No. 11, November, 2015)

ORIENTATION DEPENDENCE OF FUNCTIONAL PROPERTIES IN HETEROPHASE SINGLE CRYSTALS OF THE $Ti_{36.5}Ni_{51.0}Hf_{12.5}$ AND $Ti_{48.5}Ni_{51.5}$ ALLOYS

E. Yu. Panchenko,[1] Yu. I. Chumlyakov,[1] N. Yu. Surikov,[1] A. I. Tagiltsev,[1] N. G. Vetoshkina,[1] K. S. Osipovich,[1] H. Maier,[2] and H. Sehitoglu[3]

UDC 669.24'295-620.181:548.55

The features of orientation dependence of stress-induced thermoelastic B2–(R)–B19′-martensitic transformations in single crystals of the $Ti_{48.5}Ni_{51.5}$ *and* $Ni_{51.0}Ti_{36.5}Hf_{12.5}$ *(at.%) alloys, which contain disperse particles of the* Ti_3Ni_4 *and H-phase, respectively, are revealed along with those of their shape-memory effects (SME) and superelasticity (SE). It is experimentally demonstrated that irrespective of the crystal structure of disperse particles measuring more than 100 nm, for their volume fraction f > 16% there is a weaker orientation dependence of the reversible strain in the cases of manifestation of SME and SE. In the orientations of Class I, wherein martensitic detwinning introduces a considerable contribution into transformation strain, the values of SME* $|\varepsilon_{SME}|$ *and SE* $|\varepsilon_{SE}|$ *decrease by over a factor of two compared to the theoretical lattice strain value* $|\varepsilon_{tr0}|$ *for a B2–B19′-transformation and the experimental values of reversible strain for quenched* TiNi *crystals. In the orientations of Class 2, wherein detwinning of the martensite is suppressed as is the case in quenched single-phase single crystals, the reversible strain is maintained close to its theoretical value* $|\varepsilon_{tr0}|$*. Micromechanical models of interaction between the martensite and the disperse particles are proposed, which account for the weaker orientation dependence of* $|\varepsilon_{SME}|$ *and* $|\varepsilon_{SE}|$ *due to suppression of detwinning of the B19′-martensite crystals by the particles and a transition from a single-variant evolution of the stress-induced martensitic transformations to a multiple-variant evolution of transformations in the cases of increased size of the particles and their larger volume fractions.*

Keywords: thermoelastic martensitic transformations, single crystals, shape memory effect, superelasticity, disperse particles.

INTRODUCTION

Within recent time, engineering of high-strength materials demonstrating shape-memory effects (SPE) and superelasticity (SE) has been especially intensive, including applications in science and technology, primarily, their use in vibration suppressing devices in the aerospace industries. Among the most common functional alloys are those based on nickel titanium with *B*2–(*R*)–*B*19′-thermoelastic martensitic transformations (MTs), which are widely applied due to a combination of large reversible strains during manifestation of SME and SE, high ductility, corrosion resistance, and biological compatibility. It is well known [1–5] that by increasing the content of Ni ($C_{Ni} \geq 50.5$ at.%) both in binary

[1]V. D. Kuznetsov Physical-Technical Institute of Tomsk State University, Tomsk, Russia, e-mail: panchenko@mail.tsu.ru; chum@phys.tsu.ru; jet_n@mail.ru; antontgl@gmail.com; vetoshkina23011991@mail.ru; osipovich_k@mail.ru; [2]Institut für Werkstoffkunde, Leibniz Universität Hannover, Garbsen, Germany, e-mail: maier@iw.uni-hannover.de; [3]Department of Mechanical Science and Engineering, University of Illinois, Urbana, USA, e-mail: huseyin@illinois.edu. Translated from Izvestiya Vysshikh Uchebnykh Zavedenii, Fizika, No. 11, pp. 47–55, November, 2015. Original article submitted July 13, 2015.

alloys, such as TiNi, and in the NiTiHf alloys, it is possible to achieve a high-strength state of the *B*2-austenite (the stresses at the onset of plastic flow in the austenite turn out to be higher than G/100, G – shear modulus) due to the deviation of the alloy composition from stoichiometry and due to dispersion hardening in the case of precipitation of a large volume fraction ($f > 7$–8%) of coherent particles during aging.

In the binary TiNi alloys during aging within the temperature interval 673–873 K, there is precipitation of disperse Ti_3Ni_4 particles, having rhombohedral atomic structure different from the *B*2-matrix, which are not subjected to MTs [1–3]. Because of the difference in the lattice parameters of the particles and the *B*2-matrix, the disperse particles become sources of internal stresses, they favor nucleation of crystals of the *R*- and *B*19′-martensite at the particle–matrix interface and determine the functional properties of the material [1–3, 6].

Doping of NiTi alloys with 10 to 30 at.% of Hf rather than titanium atoms in the vicinity of an equiatomic composition (C_{Ni} = 49.0–50.0 at.%) results in increased MT temperatures and allows designing high-temperature shape memory alloys. In the $Ni_{49.0}Ti_{21}Hf_{30}$ alloy, the temperature of the onset of a *B*2–*B*19′ MT (M_s) during cooling is as high as 525 °C [7]. Low strength properties of the *B*2-austenite in TiNi alloys with the Ni content less than 50 at.% favor degradation of their functional properties under cyclic stresses, therefore, as far as high strength is concerned there is an increased interest in TiNiHf alloys containing more than 50.5 at.% of Ni. The literature on high-nickel TiNiHf alloys reports precipitation of both rhombohedral Ti_3Ni_4 particles [8] and FCC orthorhombic H-phase particles during aging [9, 10]. So far no systematic investigations have been performed of either the aging processes or the effect of disperse particles on SME and SE in TiNiHf containing more than 50.5 at.% Ni.

The purpose of this work is to identify peculiar features of the orientation dependence of stress-induced thermoelastic MTs, SME, and SE in single crystals of $Ni_{51.0}Ti_{36.5}Hf_{12.5}$ and $Ti_{48.5}Ni_{51.5}$ (at.%) alloys in stress, which contain disperse particles measuring more than 100 nm.

The use of single crystals for investigations offers a possibility of studying the orientation dependence of SME and SE, and, using selected orientations, would allow us to vary strength properties of the high-temperature phase and critical stresses of the martensite formation without changing the microstructure and chemical composition of the crystals. By using single crystals, we can rule out both the influence of grain boundaries on the evolution of MTs and particle distribution and to clarify the role of the high-strength state of the austenite in the formation of functional properties of the material.

For this study we primarily selected the orientations characterized by the maximum and minimum theoretically calculated lattice deformation values in the course of the *B*2–*B*19′-martensitic transformations: $\varepsilon_{tr0}^{[122]}/\varepsilon_{tr0}^{[001]} = 3.7$ for $Ti_{48.5}Ni_{51.5}$-single crystals and $\varepsilon_{tr0}^{[236]}/\varepsilon_{tr0}^{[001]} = = 4.8$ for $Ni_{51.0}Ti_{36.5}Hf_{12.5}$ crystals. Single crystals of $Ti_{48.5}Ni_{51.5}$ were investigated by tensile deformation, since these crystals in compression in the course of *B*2–*B*19′ MTs are characterized by a week orientation dependence $\varepsilon_{tr0}^{[122]}/\varepsilon_{tr0}^{[001]} = 1.2$ in contrast to $Ni_{51.0}Ti_{36.5}Hf_{12.5}$-crystals investigated in compression. Second, we used so-called *hard* orientations near the [001]-direction, which in TiNi crystals exhibit high strength because of Schmidt's factors (m) approximating zero for the operative slip systems <100> {110}, and so-called *soft* orientations in the vicinity of the [$\bar{1}$ 11]-direction (m = 0.47).

1. EXPERIMENTAL PROCEDURE

Single crystals of $Ni_{51.0}Ti_{36.5}Hf_{12.5}$,$Ti_{49.0}Ni_{51.0}$ and $Ti_{48.5}Ni_{51.5}$ (at.%) alloys were grown using the Bridgeman's process in an inert gas atmosphere in a graphite crucible. Their single-crystal structure was verified by X-ray methods and optical microscopic investigations of the crystal surface. Orientation of the specimens was determined in an X-ray DRON-3 diffractometer using FeK_α-emission. To achieve single-phase state, the single-crystal specimens of $Ti_{48.5}Ni_{51.5}$ and $Ti_{49.0}Ni_{51.0}$ measuring 3.0×1.5×16 mm were homogenized at 1173 K during 20 hours in an inert-gas atmosphere and quenched into water at room temperature after annealing in helium at 1203 K for 0.5 hour. Single-crystal $Ni_{51.0}Ti_{36.5}Hf_{12.5}$ specimens were investigated in the as-grown heterophase state. Prior to testing, the specimens were ground and polished in a 5% $HClO_4$ + 95% CH_3COOH electrolyte at T = 293 K, U = 22 V. Aging of single crystals of $Ti_{48.5}Ni_{51.5}$ was performed at T = 823 K for t= 1.5 h in a quartz tube in a helium medium followed by quenching into water.

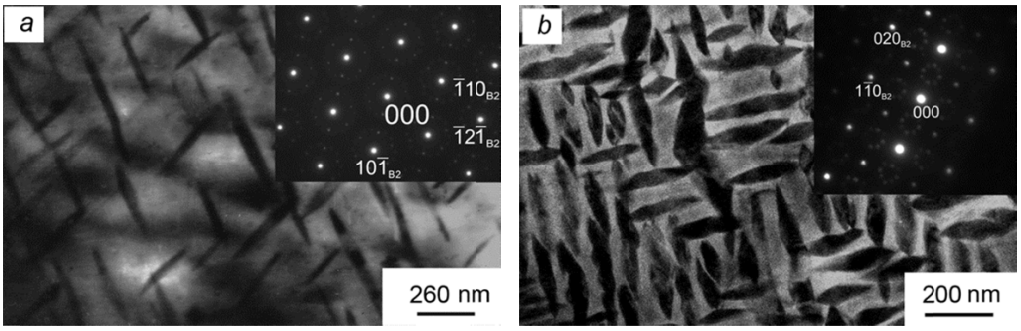

Fig. 1. Microstructure of single-crystal $Ti_{48.5}Ni_{51.5}$ specimens aged at 823 K/1.5 h, zone axis $[111]_{B2}$, the orientation dependence fulfilled is as follows: $(\bar{1}10)_{B2} \parallel (300)_R \parallel (3\bar{2}\bar{1})_{Ti_3Ni_4}$ (*a*) and as-grown heterophase $Ni_{51.0}Ti_{36.5}Hf_{12.5}$ single crystals, zone axis $[001]_{B2} \parallel [100]_{H\text{-phase}}$ (*b*).

The starting and final temperatures of the forward and reverse *B*2(*R*)–*B*19′ MTs, (M_s, M_f) and (A_s, A_f), respectively, were determined from variations in the electrical conductivity of the specimens within the heating-cooling cycle. The aged $Ti_{48.5}Ni_{51.5}$ single crystals undergo a *B*2–*R*–*B*19′ MT with the characteristic temperatures being: T_R = 285(±2) K (T_R – the onset temperature for a *B*2–*R*–*B*19′ MT during cooling), M_s = 224(±2) K and A_f = 285(±2) K. In single crystals of the $Ni_{51.0}Ti_{36.5}Hf_{12.5}$ alloy, the *B*2–*B*19′ MT temperatures are found to be M_s = 190(±2) K and A_f = 235(±2) K.

Microstructure of these single crystals was investigated in the Philips CM 200 and JEOL 2010 transmission electron microscopes at the accelerating voltage 200 kV. Mechanical tests were performed in an Instron 5969 universal testing machine at the strain rate $\dot{\varepsilon} = 2 \cdot 10^{-3}$ 1/s.

2. EXPERIMENTAL RESULTS AND DISCUSSION

Figure 1 presents TEM images of microstructure of heterophase $Ti_{48.5}Ni_{51.5}$ and $Ni_{51.0}Ti_{36.5}Hf_{12.5}$ single crystal specimens. Aging of $Ti_{48.5}Ni_{51.5}$ single crystals at 823 K for 1.5 h without loading results in precipitation of four crystallographically equivalent variants of lens-like Ti_3Ni_4 particles having the lengths within d = 380–430 nm and the habitus plane of the $\{111\}_{B2}$ type (Fig. 1*a*). The disperse particles measuring up to 430 nm remain coherently bound with the matrix. TEM examinations reveal a strain-induced contrast near the particles, and there are no defects at the particle–matrix interface. This is consistent with the literature data [1, 2, 11]. The authors of [11] found that the particle lost coherence no sooner than they became as large as 1000 nm and at the particle–matrix interface there appeared dislocations with the Burgers vectors along the $<111>_{B2}$- and $<100>_{B2}$-directions, which eliminated the mismatch between the particle and matrix lattices. The volume fraction of the particles was $f \sim (16.0 \pm 0.5)\%$. A similar volume fraction of disperse particles, f = 14–20%, was reported in $Ti_{48.7}Ni_{51.3}$ crystals in the course of aging at 773–823 K in [12]. Moreover, it was experimentally found that in as-grown $Ni_{51.0}Ti_{36.5}Hf_{12.5}$ single crystals during their slow cooling, there was a large (up to 30%) volume fraction of the H-phase precipitates measuring (140 ± 20) nm in length (Fig. 1*b*), which was also reported in [13]. These H-phase precipitates were reported to have an orthorhombic lattice and a chemical composition of $Ni_{0.52}Ti_{0.19}Hf_{0.29}$ [9, 10]. In the microdiffraction patterns from their specimens, there were evident satellite reflections, $1/4[210]_{B2}$ and $1/3[110]_{B2}$, from the four crystallographic variants of particles, which are typical for the H-phase precipitates. No disperse Ti_3Ni_4 particles were found in the $Ni_{51.0}Ti_{36.5}Hf_{12.5}$ single crystal specimens.

Presented in Figs. 2–5 are the results of investigation of the orientation dependence of functional properties – SME and SE, in the single crystals under study. An analysis of these data reveals common features of stress-induced thermoelastic *B*2–*B*19′ MTs in heterophase $Ti_{48.5}Ni_{51.5}$ and $Ni_{51.0}Ti_{36.5}Hf_{12.5}$ crystals containing a large volume fraction (f = 16–30%) of disperse particles whose size exceeds 100 nm. First, completely reversible *B*2–*B*19′ MTs are observed at high external axial stresses up to 1600–1700 MPa in $Ni_{51.0}Ti_{36.5}Hf_{12.5}$ crystals and at the stresses up to 800–900 MPa

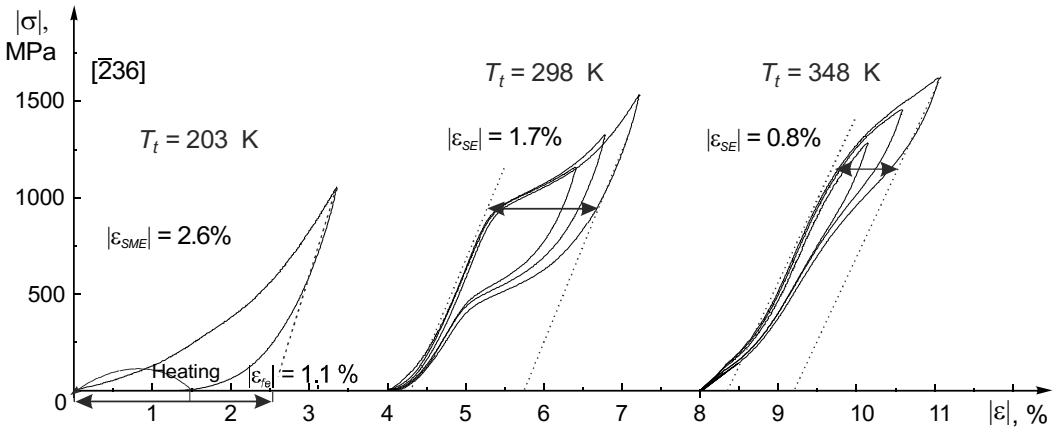

Fig. 2. Compressive stress-strain responses, σ(ε), for [$\bar{2}$ 36]-oriented $Ni_{51.0}Ti_{36.5}Hf_{12.5}$ single crystals.

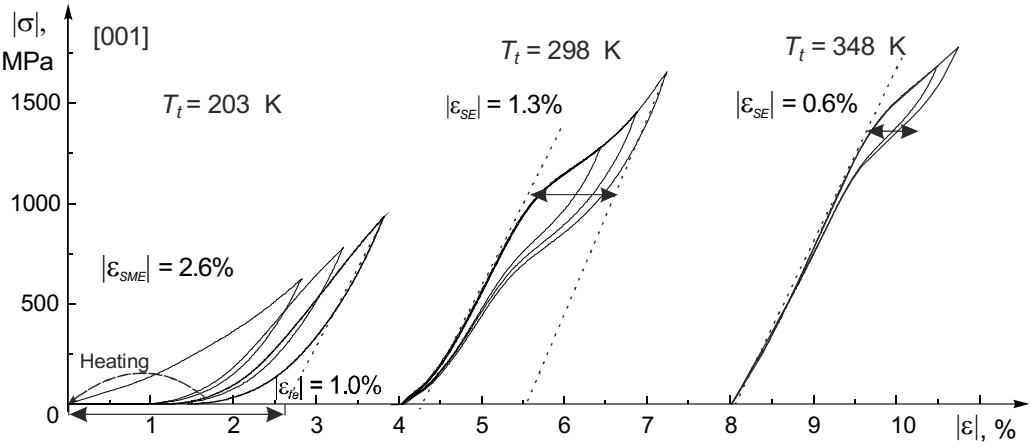

Fig. 3. Compressive stress-strain responses, σ(ε), for [001]-oriented $Ni_{51.0}Ti_{36.5}Hf_{12.5}$ single crystals.

in TiNi crystals irrespective of their orientations (Figs. 2–5). On the other hand, in TiNi poly- and single crystals containing less than 51.0 at.% of Ni in the quenched and aged states at the axial stresses between 500–700 MPa the martensite achieves its yield strength, and superelasticity is accompanied by irreversible strains [1, 3, 14, 15]. Exceptions from the above are high-strength [001]-TiNi single crystals in compression with the content of Ni more than 51.5% [16]. In single-crystal CoNiAl and NiFeGa(Co) alloys, undergoing $B2$–$L1_0$-transformations, high-temperature SE is observed up to 673 K, but the level of axial stresses strongly depends on orientation of these single crystals and they do not exceed 400 MPa in the single-phase state and 800 MPa in the aged [001]-single crystals of CoNiAl in compression [14, 15, 17, 18]. Thus, heterophase $Ti_{48.5}Ni_{51.5}$ and $Ni_{51.0}Ti_{36.5}Hf_{12.5}$ single crystals could be viewed as high-strength crystals with thermoelastic MTs.

Second, it was experimentally found that the σ(ε) curves from the crystals, irrespective of the crystallographic structure of the particles and orientation of the specimens in the course of evolution of pseudoplastic strain due to re-orientation of the martensite variants and stress-induced thermoelastic martensitic transformations, are characterized by a high strain-hardening coefficient $\theta = \delta\sigma/\delta\varepsilon$ (Figs. 2–5). In single-phase and heterophase TiNi single- and polycrystals (C_{Ni} < 51.0 at.%), containing Ti_3Ni_4 particles measuring less than 50 nm, a stress-induced MT appears as a localized Luders-type band and occurs from $\theta \to 0$ [15].

Third, the experimental values of SME and SE in $Ti_{48.5}Ni_{51.5}$ and $Ni_{51.0}Ti_{36.5}Hf_{12.5}$ crystals depend but weakly on crystal axis orientation of the crystals (Figs. 2–5, Table 1), while in quenched $Ti_{49.0}Ni_{51.0}$ crystals there is

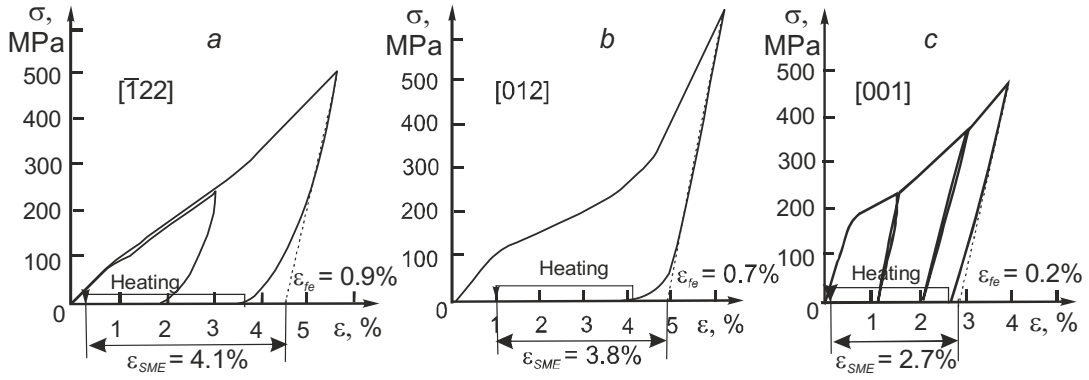

Fig. 4. Tensile stress-strain responses, σ(ε), at the test temperature T_t = 203 K < M_s for SME demonstrated in $Ti_{48.5}Ni_{51.5}$ single crystals aged at 823 K, for 1.5 h (M_s= 224 K) as a function of orientation: [$\bar{1}$ 22] (*a*), [012] (*a*), and [001] (*c*).

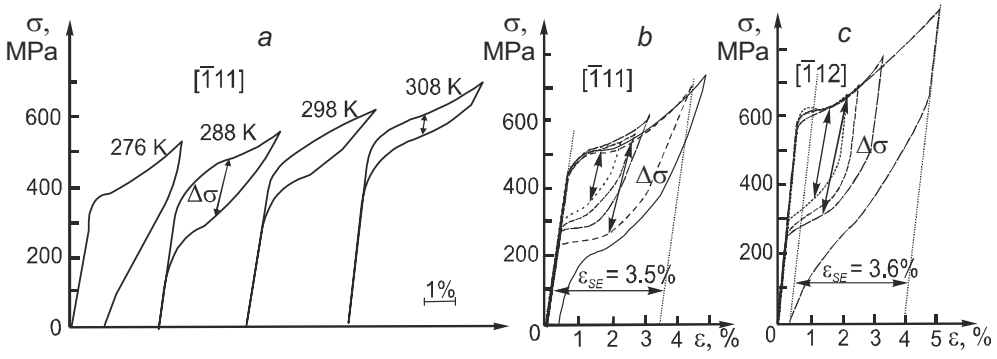

Fig. 5. Tensile stress-strain responses, σ(ε), for $Ti_{48.5}Ni_{51.5}$ single crystals aged at 823 K, for 1.5 h within the temperature interval of SE observation (A_f = 285 K): as a function of the experimental temperature (T_t) in the [$\bar{1}$ 11]-oriented crystals (*a*) and as a function of the degree of strain preset for the [$\bar{1}$ 11] and [$\bar{1}$ 12]-oriented crystals at T_t = 290 K (*b*).

an experimentally observed strong dependence of the SME value on the crystal axis orientation $|\varepsilon_{tr0}|^{[122]}/|\varepsilon_{tr0}|^{[001]} = 3.8$ (Table 1). A theoretical calculation of lattice deformation during the *B*2–*B*19′ MT both in TiNi and TiNiHf single crystals predicts a strong orientation dependence of the transformation strain (Table 1). In particular, in $Ni_{51.0}Ti_{36.5}Hf_{12.5}$ single crystals in compression, the theoretical calculations of lattice deformation during the *B*2–*B*19′ MT [1] predict a strong orientation dependence: $|\varepsilon_{tr0}|^{[236]} = 7.2\%$ and $|\varepsilon_{tr0}|^{[001]} = 1.5\%$ (Table 1). In the calculations, use was made of the averaged lattice parameters for the phases, which were determined for Ni-rich heterophase TiNiHf alloys in [19]: a_{B2} = 0.309 nm, $a_{B19'}$ = 0.3043 nm, $b_{B19'}$ = 0.4082 nm, $c_{B19'}$ = 0.4856 nm, and $\beta_{B19'}$ = 103.5°. The experimental values of SME in $Ni_{51.0}Ti_{36.5}Hf_{12.5}$ crystals were found to be $|\varepsilon_{SME}| = 2.6(\pm0.3)\%$ irrespective of the crystal orientation. It should be noted that only (1.5 ± 0.3)% of the strain predetermined for manifestation of SME is reversible after stress removal and heating up to $T > A_f$, and a considerable fraction of the predetermined inelastic strain, up to 1.1%, is reversible during unloading of the specimen (Figs. 2 and 3). This effect – spontaneous reversible inelastic strain in the σ(ε) curves during unloading of the specimen in the martensitic state due to a reverse motion of twin boundaries in the martensite, is referred to as ferroelasticity ε_{fe} [3].

Thus, in heterophase [236]-oriented $Ni_{51.0}Ti_{36.5}Hf_{12.5}$ crystals, the experimental values of transformation strain $|\varepsilon_{SME}|$, including the value of $|\varepsilon_{fe}|$, are by a factor of three lower than the theoretical values of lattice strain $|\varepsilon_{tr0}|$ under conditions of a *B*2–*B*19′ MT (Table 1). In [001]-oriented $Ni_{51.0}Ti_{36.5}Hf_{12.5}$ single crystals, on the contrary, the

TABLE 1. Orientation Dependence of Theoretically Calculated and Experimental Reversible Strain Values during Thermoelastic *B*2–*B*19′ MTs in TiNi(Hf) Crystals

Chemical composition (at.%) and heat treatment	Orientation and method of deformation*	Theoretical reversible strain values during *B*2–*B*19′ MT				Experimental values		
		$\lvert\varepsilon_{tr0}\rvert$, %	$\lvert\varepsilon_{tr0}'\rvert$, %	$\lvert\varepsilon_{CVP}\rvert$, % [20]	$\lvert\varepsilon_{CVP+detw}\rvert$, % [20]	$\lvert\varepsilon_{SME}\rvert$, %, ±0.3%	$\lvert\varepsilon_{fe}\rvert$, %, ±0.3%	$\lvert\varepsilon_{SE}\rvert$, %, ±0.3%
$Ti_{49.0}Ni_{51.0}$, Single-phase state	[$\bar{1}$ 22] T	10.7	–	6.9	11.2	10.3	1.5	–
	[001] T	2.9	–	2.7	2.7	2.7	0.5	–
$Ti_{48.5}Ni_{51.5}$, *B*2-phase + Ti_3Ni_4 particles measuring (400 ± 20) nm, *f* = (16 ± 0.5)%	[$\bar{1}$ 22] T	10.7	9.0	6.9	11.2	4.1	0.9	3.6
	[012] T	7.5	6.3	4.8	7.5	3.8	0.7	3.2
	[$\bar{1}$ 12] T	9.6	8.0	6.2	9.7	4.0	0.4	3.6
	[$\bar{1}$ 11] T	9.8	8.2	5.9	10.3	4.3	1.6	3.5
	[001] T	2.9	2.4	2.7	2.7	2.7	0.5	2.7
$Ti_{48.5}Ni_{51.0}Hf_{12.5}$, *B*2-phase + H-phase particles measuring (140 ± 20) nm, *f* = (30 ± 2)%	[$\bar{2}$ 36] C	7.2	5.0	–	–	2.6	1.1	1.7
	[001] C	1.5	1.0	–	–	2.6	1.0	1.3

*T – tension, C – compression.

experimental values of transformation strain $\lvert\varepsilon_{SME}\rvert$ are nearly twice higher than the theoretical ones $\lvert\varepsilon_{tr0}\rvert$ due to ferroelasticity $\lvert\varepsilon_{fe}\rvert$. The value of reversible strain for the cases of SE, observed under high axial deforming stresses higher than 700 MPa, in $Ni_{51.0}Ti_{36.5}Hf_{12.5}$ single crystals weakly depends on orientation and is found to be $\lvert\varepsilon_{SE}\rvert$ = (1.7 ± 0.3)% and $\lvert\varepsilon_{SE}\rvert$ = (1.3 ± 0.3)% in the [236]-oriented and [001]-oriented crystals, respectively. Relying on the analysis of the experimental values of SME and SE, one can single out two classes of orientations in $Ni_{51.0}Ti_{36.5}Hf_{12.5}$ single crystals. In Class 1, in the [$\bar{2}$ 36]-oriented crystals, the experimental values of SE $\lvert\varepsilon_{SE}\rvert$ are by a factor of 4.2 lower than the theoretical estimates of transformation strain $\lvert\varepsilon_{tr0}\rvert$ = 7.2%, while in Class 2 in the [001]-oriented $Ni_{51.0}Ti_{36.5}Hf_{12.5}$ crystals, the values of $\lvert\varepsilon_{SE}\rvert$ are close to the theoretical lattice strain values under conditions of a *B*2–*B*19′ MT $\lvert\varepsilon_{tr0}\rvert$ = 1.1% (Table 1).

Similarly to the above, in $Ti_{48.5}Ni_{51.5}$ single crystals in orientations of Class 1 ([$\bar{1}$22], [$\bar{1}$12], [$\bar{1}$11], [012]), the experimental values of transformation deformation during observation of SME and SE were found to be by a factor of 2–2.5 lower than the theoretical values of lattice deformation $\lvert\varepsilon_{tr0}\rvert$ during a *B*2–*B*19′ MT (Figs. 4 and 5, Table 1). To calculate $\lvert\varepsilon_{tr0}\rvert$, use was made of the lattice phase parameters a_{B2} = 0.30107 nm, $a_{B19'}$ = 0.2882 nm, $b_{B19'}$ = 0.4128 nm, $c_{B19'}$ = 0.4623 nm, and $\beta_{B19'}$ = 96.7°, which were determined in [20] for Ni-rich TiNi alloys. The value of ε_{tr0} for $Ti_{48.5}Ni_{51.5}$ single crystals coincide with the earlier calculations of lattice strain performed for TiNi alloys [1]. In Class 2 orientations, wherein we can single out the [001]-orientation, the values $\lvert\varepsilon_{tr0}\rvert$ = 2.7% and $\lvert\varepsilon_{SME}\rvert$ = (2.7 ± 0.3)% coincide (Fig. 4*c*, Table 1). In the [001]-oriented $Ti_{48.5}Ni_{51.5}$ crystals, unlike the [001]-oriented $Ni_{51.0}Ti_{36.5}Hf_{12.5}$ crystals, the contribution from ε_{fe} tends to zero (Fig. 4*c*). The $\sigma(\varepsilon)$ curves for the cases of observation of SE in $Ti_{48.5}Ni_{51.5}$ single crystals in tension are presented in Fig. 5. The value of reversible strain during observation of SE is virtually independent of crystal orientation and is no more than $\lvert\varepsilon_{SE}\rvert$ = (3.5 ± 0.3)% in the [$\bar{1}$ 11]-oriented $Ti_{48.5}Ni_{51.5}$ crystals, for which the theoretically calculated transformation strain is more than a factor of 2.5 higher, $\lvert\varepsilon_{tr0}\rvert$ = 9.8% (Table 1). In the single crystals under study, the value of stress hysteresis $\Delta\sigma$, characterizing the value of energy dissipation during reversible thermoelastic MTs, is determined by the experimental temperature and the value of reversible strain (Fig. 2, 3, 5). First, the value of $\Delta\sigma$ decreases with increasing the experimental temperature, which is typical for high-strength poly- and single crystals exhibiting SE in a quite wide temperature interval [15, 17]. Second, $\Delta\sigma$ increases with the value of predetermined strain in the loading – unloading cycle, which was demonstrated earlier for $Ti_{48.5}Ni_{51.5}$ crystals aged in compression at 823 K for 1.5 h [16].

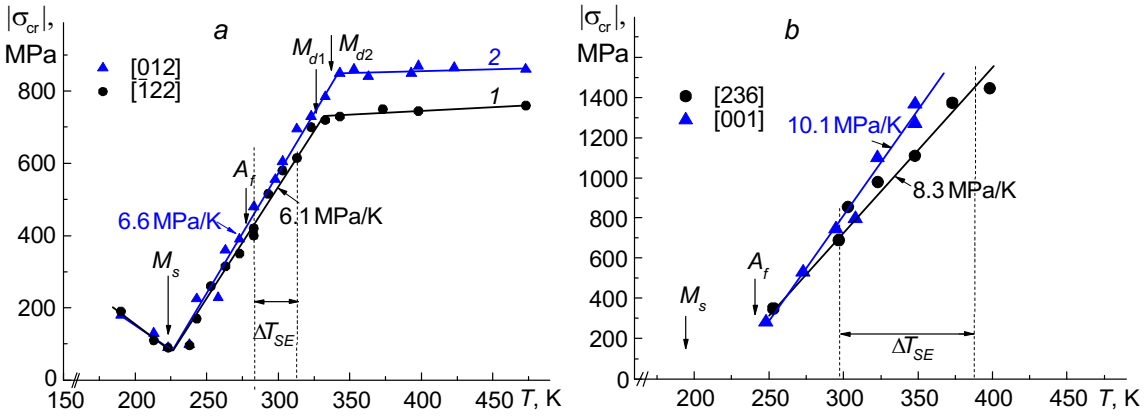

Fig. 6. Temperature dependence of critical stresses for $Ti_{48.5}Ni_{51.5}$ single crystals in tension, aged at 823 K/1.5 h (*a*) and heterophase $Ti_{36.5}Ni_{51.0}Hf_{12.5}$ single crystals in compression (*b*).

The dependence of axial critical stresses of martensite formation on the experimental temperature for $Ni_{51.0}Ti_{36.5}Hf_{12.5}$ and $Ti_{48.5}Ni_{51.5}$ crystals is presented in Fig. 6. It is evident that the critical stresses, necessary for the onset of a *B*2–*B*19′ MT at $T>M_s$, increase following the Clausius–Clapeyron relation

$$d\,|\,\sigma_{cr}\,|/dT = -\Delta S/\varepsilon_{tr}\,. \qquad (1)$$

Here ε_{tr} is the transformation strain and ΔS is the variation in entropy during an MT.

In contrast to single-phase and aged TiNi(Hf) single crystals containing nanosized particles, the experimental values of $\alpha = d|\sigma_{cr}|/dT$ within the temperature interval of a stress-induced MT are close for all orientations in the heterophase crystals and are found to be: α = 8.3–10.1 MPa/K for $Ni_{51.0}Ti_{36.5}Hf_{12.5}$ crystals and α = 6.1–6.3 MPa/K for $Ti_{48.5}Ni_{51.5}$ crystals (Fig. 6). Similar values, α = 6.5 MPa/K, were observed for the [001]-oriented $Ti_{48.5}Ni_{51.5}$ crystals in compression aged at 823 K for 1.5 h [16]. As follows from Eq. (1), degeneration of the orientation dependence of critical stresses (σ_{cr}) of martensite formation is due to the absence of any orientation dependence of the reversible strain during observation of SME $|\varepsilon_{SME}|$ and SE $|\varepsilon_{SE}|$ (Table 1). The temperature interval of SE observation (ΔT_{SE}) also hardly depends on crystal orientation and is found to be ΔT_{SE} ~ 35 K in $Ti_{48.5}Ni_{51.5}$ crystals, while in $Ni_{51}Ti_{36.5}Hf_{12.5}$ single crystals it is twice larger (ΔT_{SE} ~ 75 K).

Thus, the peculiar manifestations of SME and SE revealed in this study, the absence of their orientation dependence in heterophase $Ti_{48.5}Ni_{51.5}$ and $Ni_{51.0}Ti_{36.5}Hf_{12.5}$ crystals do not depend on the crystallographic structure of disperse particles and chemical composition of single crystals, but are primarily determined by the level of strength properties of the high-temperature *B*2-phase and the size and volume fraction of disperse particles, which are not subjected to thermoelastic MTs.

In Class 1 orientations ([$\bar{1}$ 11], [$\bar{1}$ 22], [$\bar{1}$ 12], [$\bar{2}$ 36], [012]) of heterophase TiNi(Hf) single crystals, there is a considerable (by a factor of 2.0–4.2) decrease in the value of reversible strain revealed during measurements of SME and SE compared to quenched TiNi crystals and theoretical lattice strain values $|\varepsilon_{tr0}|$ (Table 1), while in Class 2 orientations ([001]) of these crystals the experimental and theoretical values of reversible strain are similar. Lower experimental values of reversible strain are due to, first, composite-induced effect – disperse Ti_3Ni_4 and H-phase particles do not undergo any MTs and, hence, a certain volume fraction of the material, f = 16% in $Ti_{48.5}Ni_{51.5}$ crystals and f= 30% in $Ni_{51.0}Ti_{36.5}Hf_{12.5}$ crystals does not contribute into transformation strain. The theoretical value of reversible strain in such crystals is lower

$$|\varepsilon_{tr0}'| = |\varepsilon_{tr0}|(1-f)\,. \qquad (2)$$

The theoretical values of $|\varepsilon_{tr0}'|$ are listed in Table 1. The values of $|\varepsilon_{tr0}|$ in Class 1 orientations are higher than those in Class 2, therefore, due to the composite-induced effect the value of reversible strain is reduced by 1.2–2.2% in orientations of the former class and by 0.5% in orientations of the latter. Thus, in the heterophase [001]-oriented TiNi(Hf) crystals (Class 2 orientations) a decrease in the experimental values of $|\varepsilon_{SME}|$ and $|\varepsilon_{SE}|$ due to the composite-induced effect is comparable to a measurement error of ±0.3% and hardly influences the value of reversible strain in contrast to the case with Class 1 orientations. Hence, $|\varepsilon_{SE}|$ and $|\varepsilon_{tr0}|$ in the [001]-oriented TiNi(Hf) crystals have close values. Second, disperse particles make reorientation and detwinning of the *B*19′-martensite crystals difficult during transformation evolution. Detwinning of the martensite crystals makes a considerable contribution into the transformation strain, up to 50%, ($|\varepsilon_{CVP}| < |\varepsilon_{CVP+detw}|$) in Class 1 orientations, and is one of primary factors of a considerable reduction in the reversible strain during manifestation of SME and SE in the heterophase [$\bar{1}$ 11]-, [$\bar{1}$ 22]-, [$\bar{1}$ 12]-, [$\bar{2}$ 36]-oriented crystals (Table 1). For the [001]-oriented crystals (Class 2 orientation) $|\varepsilon_{CVP}| = |\varepsilon_{CVP+detw}|$, hence, this factor does not affect the value of reversible strain. Third, we cannot entirely rule out the fact that in the case of a high volume fraction of disperse particles it is very likely that not the entire volume of the *B*2-matrix is involved in the transformation. There might be regions in the crystals with small interparticle spacing less than 50 nm (Fig. 1*b*), which do not undergo any transformation due to the size effect [22]. The third factor might strongly contribute into reduction of reversible strain in $Ni_{51.0}Ti_{36.5}Hf_{12.5}$ single crystals with a large volume fraction of particles, up to 30%, compared to that in $Ti_{48.5}Ni_{51.5}$ crystals (f= 16%).

An analysis of the σ(ε) curves allows us to determine the ratio between contributions from the dissipated ΔG_{fr} and reversible ΔG_{rev} energy during an MT, using the relation for critical stresses during a stress-induced MT at a constant temperature (σ_{Ms}, σ_{Mf}, σ_{As}, σ_{Af}) [23]

$$\sigma_{M_s}(T) = \sigma_0(T) + \frac{|\Delta G_{fr}(0)| + |\Delta G_{rev}(0)|}{\varepsilon_{tr}},\ \sigma_{M_f}(T) = \sigma_0(T) + \frac{|\Delta G_{fr}(1)| + |\Delta G_{rev}(1)|}{\varepsilon_{fr}},$$

$$\sigma_{A_s}(T) = \sigma_0(T) - \frac{|\Delta G_{fr}(1)| - |\Delta G_{rev}(1)|}{\varepsilon_{fr}},\ \sigma_{A_f}(T) = \sigma_0(T) - \frac{|\Delta G_{fr}(0)| - |\Delta G_{rev}(0)|}{\varepsilon_{fr}}. \quad (3)$$

Here $\Delta G_{rev}(0)$ and $\Delta G_{rev}(1)$ is the reversible component of non-chemical free energy characterizing the elastic and surface energy accumulated in the material in the course of evolution of an MT for the volume fractions of martensite $\delta \to 0$ and $\delta \to 1$, respectively, $\Delta G_{fr}(0)$, $\Delta G_{fr}(1)$ is the irreversible component of non-chemical free energy characterizing the energy dissipation during an MT. All values of ΔG_{rev} and ΔG_{fr} are written per unit molar volume of the alloy. Stress $\sigma_0(T)$ can be determined as $\sigma_0(T) = -\Delta S(T - T_0)/\varepsilon_{tr}$ [23].

In the heterophase crystals under study, containing large particles measuring $d > 100$ nm, deformation in the σ(ε) curves develops with a high strain hardening coefficient θ and is accompanied by an increased stress hysteresis Δσ with an increasing strain degree (Figs. 2–5). In this case, it is the particles measuring $d > 100$ nm which are preferential sites of nucleation of martensite crystals, which under the action of external stresses results in the formation of *oriented* and *nonoriented* martensite.

– Oriented martensite is the martensite formed following the application of an external stress in the systems with the Schmidt's factor maximum for a *B*2–*B*19′ MT.

– Nonoriented martensite is generated by the elastic fields from disperse particles and its orientation in the general case does not coincide with that of the martensite crystals being formed in the external stress field.

In the course of aging in a free state, a number of crystallographically equivalent variants of disperse particles are formed in the crystals (4 variants of Ti_3Ni_4 particles [1, 2] and 6 variants of H-phase particles [9, 10]), which in turn favor nucleation of different variants of martensite, which are oriented in accordance with the local stress fields at the particle–matrix interface, which is supported by the electron microscopy investigations [6, 12]. Therefore, martensite in the aged crystals with particles measuring $d > 100$ nm possesses a multivariant structure. The evolution of strain with a high strain hardening coefficient θ results from multiple nucleation of martensite crystals, their interaction with each other and hindering of the processes of their coalescence due to the presence of disperse particles. The mechanical conditions, stress field, and geometry in the vicinity of the martensite – austenite boundaries considerably change in the

course of an MT under stress with an increase in the size and number of martensitic plates, which gives rise to an increased stress hysteresis $\Delta\sigma$ with increasing degree of predetermined strain during evolution of an MT under stress. Hence it follows from Eq. (3) that an increase in the stresses with increasing volume fraction of martensite, which are necessary for an MT to develop, is due to both reversible energy accumulation and increased energy dissipation

$$(\sigma_{M_f} - \sigma_{M_s})\varepsilon_{\text{fr}} = (|\Delta G_{\text{rev}}(1)| - |\Delta G_{\text{rev}}(0)|) + (|\Delta G_{\text{fr}}(1)| - |\Delta G_{\text{fr}}(0)|) . \quad (4)$$

As a result, this multivariant morphology of martensite becomes independent of crystal orientation and is controlled by the parameters of microstructure. This gives rise to a weaker orientation dependence of SME and SE compared to a single-phase state. In single-phase TiNi single crystals there are no conditions for formation of nonoriented martensite and there is a strong orientation dependence of the value of SME, which corresponds to the theoretical value of lattice strain during a *B*2–*B*19′ MT (Table 1). Thus in heterophase TiNi(Hf) single crystals, containing disperse particles measuring more than 100 nm, an idea of a natural nanocomposite with SME is realized, where the processes of nucleation and distribution of martensite crystals are controlled by the interparticle distance. All characteristic parameters of the initial microstructure and martensite crystals have dimensions lying within ~100–400 nm.

SUMMARY

It has been experimentally shown that in heterophase $Ti_{48.5}Ni_{51.5}$ single crystals in tension and $Ni_{51.0}Ti_{36.5}Hf_{12.5}$ crystals in compression, which contain large fractions (f > 15%) of disperse particles (of Ti_3Ni_4 and H-phase) measuring d > 100 nm, the following peculiar features of manifestation of SME and SE are observed irrespective of crystallographic structure and chemical composition:

– weaker orientation dependence of critical stresses of martensite formation, SME and SE;

– considerably decreased reversible strains during SME and SE, a factor of 2.0–4.2 lower than the theoretical estimates of transformation strain $|\varepsilon_{tr0}|$ in Class 1 orientations, for which a significant contribution into transformation strain comes from detwinning of the martensite crystals;

– development of inelastic deformation during an MT with a high strain hardening coefficient $\theta = \delta\sigma/\delta\varepsilon$;

– increased stress hysteresis $\Delta\sigma$ with an increase in the volume fraction of the stress-induced martensite.

This is controlled by the multivariant character of the development of a martensitic transformation due to preferential nucleation of crystals of the *B*19′-martensite near the particle–matrix boundaries. The formation of unoriented martensite during development of an MT, which is generated by the elastic fields from the particles of several crystallographic variants and hindering of its reorientation and detwinning under the action of external stresses, gives rise to lower reversible strains during observation of SME and SE, larger energy dissipation with increasing volume fraction of martensite, and higher values of the strain hardening coefficient θ in the $\sigma(\varepsilon)$ curves in the course of development of reversible stress-induced MTs.

This study has been performed using a financial support from the Russian Science Foundation within the framework of the research project No. 14-29-00012.

REFERENCES

1. K. Otsuka and X. Ren, Prog. Mater. Sci., **50**, 511–678 (2005).
2. V. G. Pushin, S. D. Prokoshkin, R. Z. Valiev, *et al*., Shape Memory Alloys. Part I. Structure, Phase Transformations and Properties [in Russian], UrB RAS (2006).
3. V. E. Gunther, V. N. Khodorenko, Yu. F. Yasenchuk, *et al*., Titanium Nickelide. New-Generation Medical Material [in Russian], Tomsk, MITS Publ. (2006).
4. S. M. Saghaian, H. E. Karaca, H. Tobe, *et al*., Acta Mater., **87**, 128–141 (2015).
5. B. C. Hornbuckle, T. T. Sasaki, G. S. Bigelow, *et al*., Mater. Sci. Eng. A, **637**, 63–69 (2015).

6. E. Yu. Panchenko, Yu. I. Chumlyakov, and H. J. Maier, Russ. Phys. J., **57**, No. 8, 100–109 (2014).
7. D. Angst, P. Thoma, and M. Kao, J. Phys. IV, **5**, C8747–C8752 (1995).
8. X. L. Meng, W. Cai, F. Chen, and L. C. Zhao, Scripta Mater., **54**, 1599–1604 (2006).
9. F. Yang, D. R. Coughlin, P. J. Phillips, *et al*., Acta Mater., **61**, 3335–3346 (2013).
10. R. Santamarta, R. Arróyave, J. Pons, *et al*., Acta Mater., **61**, 6191–6206 (2013).
11. J. Zhang, W. Cai, X. Ren, *et al*., Mater. Trans. JIM, **40**, No. 12, 1367–1375 (1999).
12. J. Michutta, Ch. Somsen, A. Yawny, *et al.,* Acta Mater., **54,** 3525–3542 (2006).
13. E. Yu. Panchenko, Yu. I. Chumlyakov, N. Yu. Surikov, *et al*., Pis'ma Zh. Tekh. Fiz., **41**, Issue 16, 68–76 (2015).
14. Yu. I. Chumlyakov, I. V. Kireeva, I. Karaman, *et al*., Russ. Phys. J., **47**, No. 9, 893–911 (2004).
15. Y. I. Chumlyakov, I. V. Kireeva, E. Y. Panchenko, *et al*., Shape Memory Alloys: Properties, Technologies, Opportunities, Switzerland, Trans. Tech. Publications Ltd. (2015).
16. H. Sehitoglu, J. Jun, X. Zhang, *et al*., Acta Mater., **49**, 3609–3620 (2001).
17. E. Panchenko, Y. Chumlyakov, H. J. Maier, *et al*., Intermetallics, **18**, 2458–2463 (2010).
18. E. Yu. Panchenko, Yu. I. Chumlyakov, H.J. Maier, *et al*., Russ. Phys. J., **55**, No. 10, 11231131 (2013).
19. A. P. Stebner, G. S. Bigelow, J. Yang, *et al*., Acta Mater., **76**, 40–53 (2014).
20. H. Sehitoglu, R. Hamilton, D. Canadinc, *et al*., Metall. Mat. Trans. A, **34**, No. 5, 6–13 (2003).
21. S. D. Prokoshkin, A. V. Korotitskiy, V. Brailovski, *et al*., Acta Mater., **52**, 4479–4492 (2004).
22. T. Waitz, V. Kazykhanov, and H. P. Karnthaler, Acta Mater., **52**, 137–147 (2004).
23. D. L. Beke, L. Daróczi, C. Lexcellent, and V. Mertinger, J. Phys. IV, **115**, 279 (2005).